



# Types of pulsating aurora: comparison of model and EISCAT electron density observations

Fasil Tesema<sup>1,2</sup>, Noora Partamies<sup>1,2</sup>, Daniel K. Whiter<sup>3</sup>, and Yasunobu Ogawa<sup>4</sup>

<sup>1</sup>Arctic Geophysics department, The University Centre in Svalbard (UNIS), Longyearbyen 9170, Norway

<sup>2</sup>Birkeland Centre for Space Science, University of Bergen, 5007 Bergen, Norway

<sup>3</sup>School of Physics and Astronomy, University of Southampton, Southampton, UK

<sup>4</sup>National Institute of Polar Research, 90-8518 Tokyo, Japan

**Correspondence:** Fasil Tesema (fasil.tesema@unis.no)

Received: 16 March 2021 – Discussion started: 29 March 2021

Revised: 15 November 2021 – Accepted: 22 November 2021 – Published: 4 January 2022

**Abstract.** Energetic particle precipitation associated with pulsating aurora (PsA) can reach down to lower mesospheric altitudes and deplete ozone. It is well documented that pulsating aurora is a common phenomenon during substorm recovery phases. This indicates that using magnetic indices to model the chemistry induced by PsA electrons could underestimate the energy deposition in the atmosphere. Integrating satellite measurements of precipitating electrons in models is considered to be an alternative way to account for such an underestimation. One way to do this is to test and validate the existing ion chemistry models using integrated measurements from satellite and ground-based observations. By using satellite measurements, an average or typical spectrum of PsA electrons can be constructed and used as an input in models to study the effects of the energetic electrons in the atmosphere. In this study, we compare electron densities from the EISCAT (European Incoherent Scatter scientific radar system) radars with auroral ion chemistry and the energetics model by using pulsating aurora spectra derived from the Polar Operational Environmental Satellite (POES) as an energy input for the model. We found a good agreement between the model and EISCAT electron densities in the region dominated by patchy pulsating aurora. However, the magnitude of the observed electron densities suggests a significant difference in the flux of precipitating electrons for different pulsating aurora types (structures) observed.

## 1 Introduction

Pulsating aurora (PsA) is a diffuse type of aurora with distinctive structures as arcs, bands, arc segments, and patches that are blinking on and off independently within a period of few seconds (Royrvik and Davis, 1977; Yamamoto, 1988). The sizes of pulsating aurora range from 10 to 200 km horizontally and 10 to 40 km vertically and usually occur at around 100 km altitude (McEwen et al., 1981; Jones et al., 2009; Hosokawa and Ogawa, 2015; Nishimura et al., 2020; Tesema et al., 2020b). Pulsating aurora is often observed after midnight, during the recovery phase of a substorm, and at the equatorward part of the auroral oval (Lessard, 2012; Nishimura et al., 2020), and it can persist for more than 2 h (Jones et al., 2011; Partamies et al., 2017; Bland et al., 2019; Tesema et al., 2020a). However, substorm growth- and expansion-phase PsA (McKay et al., 2018), as well as after-noon PsA (Berkey, 1978), have also been reported.

The latitude of pulsating aurora can span a wide range, which depends on the geomagnetic activity and local time. In general, PsA is often observed between 56 and 77° of magnetic latitude (Grono and Donovan, 2020; Oguti et al., 1981). During the post-midnight period, it is restricted to between 60 and 70° magnetic latitude, and in the morning sector, it moves to higher latitudes between 65 and 75°. The source location of these regions maps to the magnetosphere between 4 and 15  $R_E$  (Grono and Donovan, 2020). PsA is very common, with an occurrence rate of about 30 % around magnetic midnight (Oguti et al., 1981) and above 60 % in the morning sector (Oguti et al., 1981; Bland et al., 2019).

The energy of the precipitating electrons during pulsating aurora spans a wide range of magnitudes, which are predominantly between 10 and 200 keV (Miyoshi et al., 2015; Tesema et al., 2020a). However, electron energies as low as 1 keV have also been reported (McEwen et al., 1981). PsA can consist of microbursts of relativistic electrons in the high-energy tail of the precipitation, which makes PsA an important magnetosphere–ionosphere (MI) coupling process in studying radiation belt dynamics (Miyoshi et al., 2020). A significant number of studies have shown that the precipitation of PsA electrons is driven by wave–particle interactions (Miyoshi et al., 2010; Nishimura et al., 2010, 2020; Kasahara et al., 2018). Recent studies further show that chorus waves play an important role in the pitch angle scattering of electrons over a wide range of energy during pulsating aurora (Nishimura et al., 2010; Miyoshi et al., 2020). Electron cyclotron harmonic (ECH) waves are also a possible candidate in causing pulsating aurora, especially at the lower end of the PsA energy spectrum (Fukizawa et al., 2018; Nishimura et al., 2020).

A recent study by Grono and Donovan (2018) categorized pulsating aurora into three different types in relation to their structural stability and motion along the ionospheric convection. Salient and persistent structures moving along the ionospheric convection belong to patchy pulsating aurora (PPA), and transient structures with no definite motion characterize amorphous pulsating aurora (APA), which are the dominant PsA types. In addition, the third category, patchy aurora (PA), consists of very persistent structure with limited pulsation at the patch edges. The energy of the electrons associated with the pulsating aurora types are different (Yang et al., 2019; Tesema et al., 2020b). From a total of 92 PsA events, Tesema et al. (2020b) compared the D-region ionization level obtained by the EISCAT (European Incoherent Scatter scientific radar system) radars for different types of PsA and suggested that PPA is the dominant type of aurora affecting the D-region atmosphere. The different categories of PsA reported in Grono and Donovan (2018) originated from different source regions of the magnetosphere, where PPA and PA mapped entirely to the inner magnetosphere, while the APA source region spanned both the inner and outer magnetosphere (Grono and Donovan, 2020). This indicates that PsA can contribute to our understanding of the radiation belt dynamics as well, despite the challenges imposed by the large spatiotemporal variation in the PsA structures.

Energetic PsA electrons can affect the chemistry of the mesosphere by the strong production of odd hydrogen, which depletes ozone in catalytic reactions (Turunen et al., 2016; Tesema et al., 2020a). As demonstrated by Tesema et al. (2020a), the softest PsA precipitation does not have chemical consequences. It was further suggested in their study that it is mainly PA and PPA that can most effectively ionize the atmosphere below 100 km.

In this study, we test an ion chemistry and energetics model, using measurements of precipitating electrons from

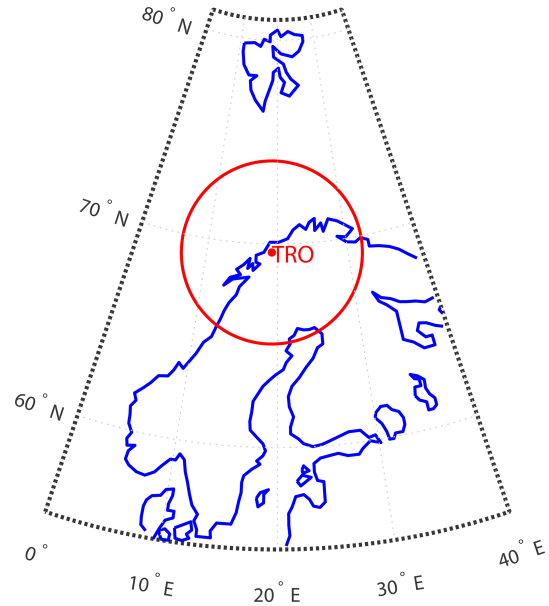


**Figure 1.** Geographic locations of the ground-based ASC station and EISCAT radars in Tromsø (TRO; red dot), Norway. The red circle marks the ASC field of view (FOV) at about 110 km altitude. Polar Operational Environmental Satellite (POES) overpasses were selected so that their footprints could be mapped to the ASC FOV.

a low-altitude satellite as an energy input. We compared the EISCAT electron density measurements with the model output electron density to investigate the ionization level during different types of pulsating aurora. This will enable us to understand the ionization rates and energy spectra, as they are measured at very different spatial and temporal resolutions, as well as the ionization changes in the transitions between different PsA types.

## 2 Data and methods

The optical data used in this study are from an all-sky camera (ASC) located in Tromsø (69.58° N, 19.21° E) in Norway (shown in Fig. 1), which is at the same site as the EISCAT radars. It belongs to the network of Watec monochromatic imagers (WMIs), which is owned and operated by the National Institute of Polar Research (NIPR). The WMI consists of a highly sensitive Watec camera, a fish eye lens, and a bandpass filter at 428, 558, and 630 nm, with a bandwidth of 10 nm. The imaging system is capable of taking images with a 1 s time resolution. In this study, we used images from the 558 nm filter. Technical details of the ASC can be found in Ogawa et al. (2020).

Measurements of precipitating electrons from an overpassing satellite, the Polar Operational Environmental Satellite (POES), are used to construct the spectrum of PsA electrons. We used corrected and calibrated POES measurements, as described in Nesse Tyssøy et al. (2016). The spectrum is used

as an input to the model discussed below. We adopted the same procedure as explained in Tesema et al. (2020a) to construct the spectrum and extrapolate the softer precipitation end using a power law function. This includes the energy range from 50 eV to 1 MeV.

Field-aligned and vertical electron density measurements are obtained from very high frequency or ultra-high frequency (VHF; UHF) EISCAT radars located in Tromsø. Instead of the standard 1 min resolution data available to the public in the EISCAT database, we use a 5 s resolution electron density processed using the GUISDAP (Grand Unified Incoherent Scatter Design and Analysis Package) software to match with the high-resolution auroral imaging. The electron density measurements of the EISCAT radars are used to compare the ionization level during the pulsating aurora, with the electron density from the model described below.

The auroral model used in this study is the combination of an electron transport code (Lummerzheim and Liliensten, 1994) and a time-dependent ion chemistry and energetics model (Palmer, 1995; Lanchester et al., 2001), which solves the coupled continuity equations for positive ions and minor neutrals above 80 km altitude.

In this study, we used the directly measured energy of precipitating electrons by POES to construct the spectrum for the input. We start the model run with an empty ionosphere since prompt precipitation below 120 km does not respond to the softer precipitation that is usually used to warm up the ionosphere for upper atmospheric studies. The runtime and time step for the model was about 3.5 and 0.2 s, respectively. The minimum and maximum altitude of the model run is 80 and 500 km, respectively. Thus, the model does not reproduce ionization below 80 km, which corresponds to 100 keV (Turunen et al., 2009).

The electron density output from the model is compared with the EISCAT-measured electron density. This will enable us to answer the question of whether the overpass-averaged spectrum is a good representative as model input or if the patchiness of the aurora should be considered in atmospheric models. Requiring the availability of EISCAT data, POES overpasses, and PsA from ASC images resulted in three events. Keograms (north–south overview) and ewograms (east–west overview) of ASC images are constructed to further classify and study the pulsating aurora structures and the associated precipitation.

### 3 Results

Pulsating aurora can easily be identified from ASC keograms (e.g., Partamies et al., 2017), and be categorized into different types using ewograms (Grono and Donovan, 2018). A keogram is created by extracting north–south pixel columns of consecutive individual all-sky images and stacking them in time, and an ewogram is an east–west counterpart of a keogram. The energy and flux of the precipitating electrons

can be inferred indirectly from the altitude and magnitude of the maximum electron density measured by ground-based incoherent scatter radars. Combining ASC data, EISCAT electron density measurements, electron density output from auroral model, and PsA energy spectra from POES measurements, we investigate the characteristics of precipitating PsA electrons and their ionization effects during three PsA events, as follows.

#### 3.1 Event 1: 17 November 2012

Figure 2 shows a keogram, ewogram, and the EISCAT electron density measurements on 17 November 2012 between 04:00 and 05:00 UT. The keogram and ewogram are generated from 1 s time resolution ASC images taken at the Tromsø EISCAT site. Before 04:27 UT, there was no electron density enhancement in the D and E regions, as there is no electron density enhancement or auroral activity during this period. After 04:27 UT, a significant electron density enhancement (more than 1 order of magnitude) is seen below 110 km. Correspondingly, the ASC data showed PsA drifting into the EISCAT field of view (FOV), where it stayed until 04:43 UT. The PsA seen during this period is dominantly the APA type. There is PPA type in the poleward region of the ASC FOV. After 04:43 UT, this PPA drifted from north to east and became visible in the EISCAT radar FOV. The APA coverage started to diminish, and the PPA took over most of the camera FOV. A clear transition in the EISCAT electron density is apparent at 04:43 UT. The electron density showed a thicker layer, and the precipitation reached deeper, below 90 km, especially after 04:49 UT. The thicker layer and more energetic precipitation corresponds to the PPA seen over the EISCAT radar.

Figure 3 shows the ASC images at 16 s intervals (Fig. 3g–k), the PsA spectrum constructed from POES measurements at the blue dots on the ASC images (Fig. 3g–l), the electron density measured by EISCAT and modeled using the POES spectra, and green line emission intensity at the EISCAT (red) and POES (blue) measurement locations. From the ASC images, it is clearly seen that the PsA structures are slowly drifting to the east, with decreasing intensity in the south (see also video 1 in the Supplement). This drift can be seen as patch lines (path lines appear with or without striations for patchy pulsating or patchy aurora, respectively; Grono et al., 2017) in the ewogram in Fig. 2. The median intensity of 10 pixels around the location of EISCAT (red) and the POES measurements (blue) are plotted in Fig. 3l. The intensity at the location of EISCAT over the entire duration was high, while at the location of the POES measurements in the last three ASC images the intensity is extremely low. Looking at the electron density comparison between the model and EISCAT radar measurements, there is a good agreement between the two (Fig. 3g–j), except for the last two panels (Fig. 3k–l), where the POES and EISCAT observations are looking into an entirely different region of auroral intensity.

The first four points of the POES observation spectra show similar magnitudes; the curves (a–e) plotted in Fig. 3f correspond to the ASC observations in Fig. 3a–e. During this period, the altitude of maximum electron density in the EISCAT measurements was 95 km, and from the model output, it was 105 km. There is no significant differences in the electron density profiles as the FOV of EISCAT is mostly looking into a patch. The POES data points were also measurements within the patch's on period, except in Fig. 3d, where there was very low emission (Fig. 3l). Even though the emission intensity was low right after the whole FOV of the camera was filled with patches (as seen in the keogram plot in Fig. 2), the electron density agreement between the model and EISCAT stayed the same in Fig. 3k. From Fig. 3d, POES is looking into a low-emission region, which has correspondingly low fluxes in the spectra, which is similar to the spectra as in Fig. 3e–f. It is also clearly evident that, above 10 keV, the flux of electrons in Fig. 3d stayed similar to the previous three ASC observations. However, for the last two ASC observations (Fig. 3e–f), the POES observations were probably outside the precipitation region as the precipitating electron energies in the spectrum plot showed a large decrease above 10 keV in Fig. 3g. This causes a huge discrepancy between the model and EISCAT electron densities, accordingly.

The spectra from POES (Fig. 3g) does not show significant variations, except for the last two spectra in time. Above 10 keV, there is a significant drop in electron flux for the last two observations (Fig. 3e–f). This corresponds to the low emission observed at those two points in the ASC images. The electron density comparison shows a good agreement between altitudes of 90 and 120 km in the first four panels. However, the last two panels show a big difference in the electron fluxes. The shape of the curves in these two panels are similar, and the gap between the curves below 80 km becomes narrower in these two panels.

The altitude of the maximum electron density showed a significant difference between the model run and the EISCAT observations. However, the magnitude of the electron density showed a good agreement between 85 and 120 km. The height of the maximum electron density for the model output is about 105 km (corresponding to 10 keV electrons), and model output of the EISCAT measurements is 95 km (corresponding to 25 keV electrons; Turunen et al., 2009). Note that the model can only reproduce the electron density above 80 km, and thus, below 90 km the discrepancy between the two densities becomes larger. The electron densities above 120 km are due to the softer precipitation and were approximated by a power law function, which may not reproduce realistic ionization in this region. In addition, we did not perform a warming up of the ionosphere (the model run started from an empty ionosphere) since we are interested in the prompt energetic electron precipitation effects below 120 km. However, comparing the region between 85 and 120 km, the model and EISCAT electron densities showed an average difference of half an order of magnitude.

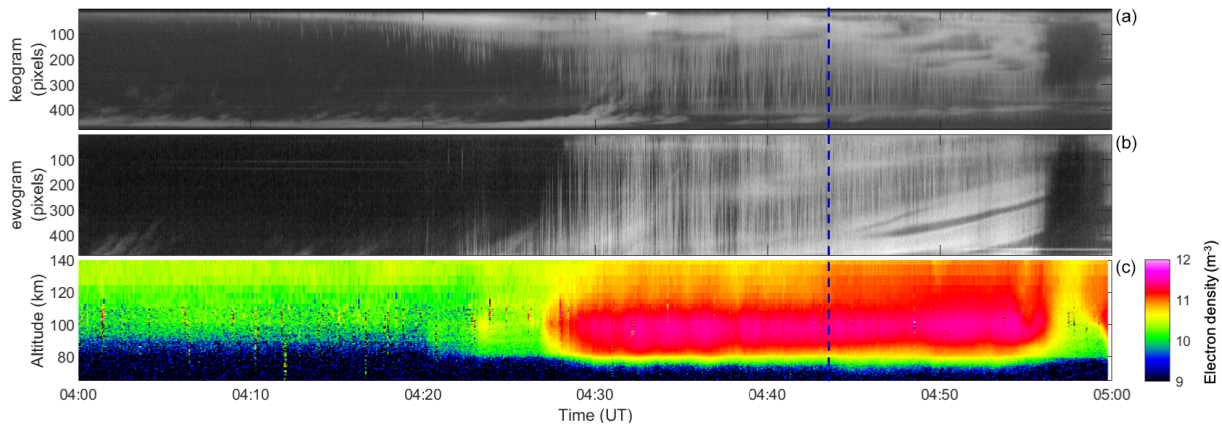
The last two panels in the electron density (Fig. 3k–l) comparison showed a kink-like structure at around 90 km, corresponding to 40 keV electrons. From the spectrum, it is apparent that, above 40 keV, the spectra for these two cases (magenta and cyan colors) showed almost the same fluxes. The median intensity around the EISCAT and satellite observations showed a large difference in these two panels (Fig. 3k–l). From the EISCAT electron density plots shown in Fig. 3h–l, the zenith (black curve) and field-aligned measurements (red curve) are similar. This event was studied by Miyoshi et al. (2015), using the same EISCAT data; however, we used different ASC data and additional satellite data and model outputs in this study.

### 3.2 Event 2: 9 November 2015

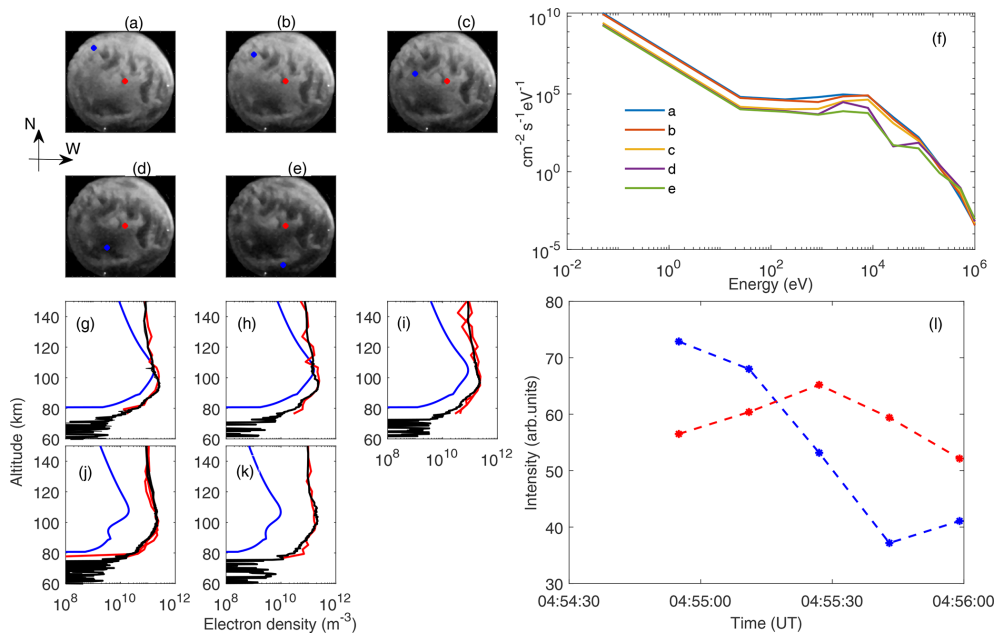
Figure 4 shows the keogram, ewogram, and EISCAT electron density measurements on 9 November 2015 between 02:00 and 03:00 UT. The keogram and ewogram are generated from 1 s time resolution ASC images in Tromsø. For this event, a mixture of PsA types is clearly seen. Before 02:24 UT, the PsA type was APA, which was followed by both APA and PPA (see also video 2 in the Supplement). During this 1 h period, the PsA structure and the magnitude of the electron density over the ASC and EISCAT FOV change significantly. After 02:24 UT, the PPA starts to emerge from the south and move northward to fill the FOV after 02:42 UT. The electron density significantly dropped between 02:04 and 02:28 UT (Fig. 4c), when the EISCAT FOV was predominantly observing the APA type. After 02:44 UT, the dominant PPA type corresponds to the increase in electron density and also deeper precipitation. It is also clearly seen that the width of the ionization layer starts to become thicker after 02:20 UT when a mix of PsA types and, later, PPA is observed over the FOV of EISCAT.

Figure 5 shows the ASC observation, the POES spectra for the overpass data points (blue dots), the electron density measurements at EISCAT (red dots in the ASC images), and the electron density from the model output (blue curve), using the spectra obtained from POES (blue dots in the ASC images). The ASC images were dominated by two different auroral structures. The poleward portion of the ASC is filled with a diffuse arc and the equatorward portion with patches. It is not clearly seen if the diffuse arc is pulsating or not. But, when displaying all images as a video (see the video Supplement), the structure over the EISCAT FOV is seen to be pulsating and can be categorized as APA. However, the POES measurements encounter a different type of PsA, namely PPA.

The spectra measured by POES are shown in Fig. 5e. The peak flux of the electrons was observed below 10 keV. Above 100 keV, data point 4 showed significantly higher fluxes compared to the others. The height difference of the maximum electron density between the model output and EISCAT observations is small. However, the fluxes show more than 1 or-



**Figure 2.** Keogram (a), ewogram (b), and EISCAT electron density as a function of height (c) from UHF radar in Tromsø on 17 November 2012 between 04:00 and 05:00 UT. The EISCAT beam points to the center of the keogram at 235 pixels and in the ewogram at 245 pixels. The electron density is displayed in a logarithmic color scale. The blue dashed vertical line is the separation between APA and PPA, based on the FOV of EISCAT.



**Figure 3.** ASC images (a–e), with spectra constructed from POES and power law extrapolation (f). The curves labeled as a–e in panel (f) are corresponding spectra to the blue point on the ASC images, with the model (blue) and EISCAT (field aligned from UHF radar in red; zenith measurements from VHF radar in black) electron densities. Panels (g–k) correspond to the ASC images in panels (a–e), with relative auroral intensities at the location of the satellite measurements as a function of time, blue dots at POES data points corresponding to (a)–(e), and red dots at EISCAT.

der of magnitude difference. The emission intensity at data point 4 and at the EISCAT observation point showed a large difference. The POES data point 4 is entirely within the PPA precipitation region, while EISCAT is looking into the APA type. Note that this data point 4 showed higher fluxes in the energy range above 100 keV.

### 3.3 Event 3: 13 January 2016

Figure 6 shows the keogram, ewogram, and electron densities on 13 January 2016 between 05:00 and 06:00 UT. From the ASC, a very slowly drifting and persistently stable structure of pulsating aurora is seen over the whole ASC FOV, including the EISCAT FOV after 05:10 UT. A clear increase in electron density is observed when the pulsating patch is on and drifting in and out of the EISCAT FOV. The pulsat-

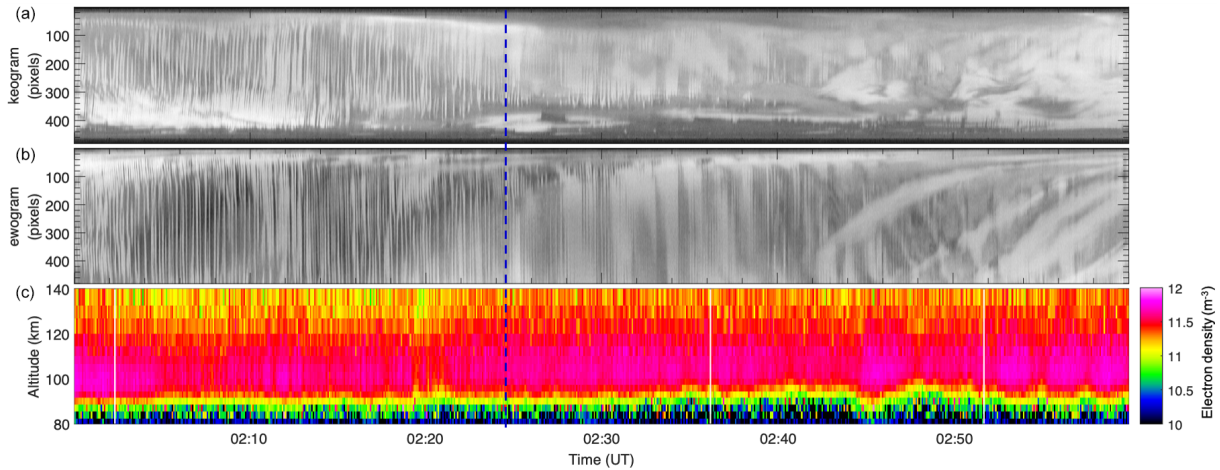


**Figure 4.** Keogram (a), ewogram (b), and EISCAT electron density (c) from UHF radar at Tromsø on 9 November 2015 between 02:00 and 03:00 UT. The EISCAT beam points to the center of the keogram at 235 pixels and in the ewogram at 230 pixels. The electron density is displayed in a logarithmic color scale. The blue dashed vertical line shows the separation between APA and PPA.

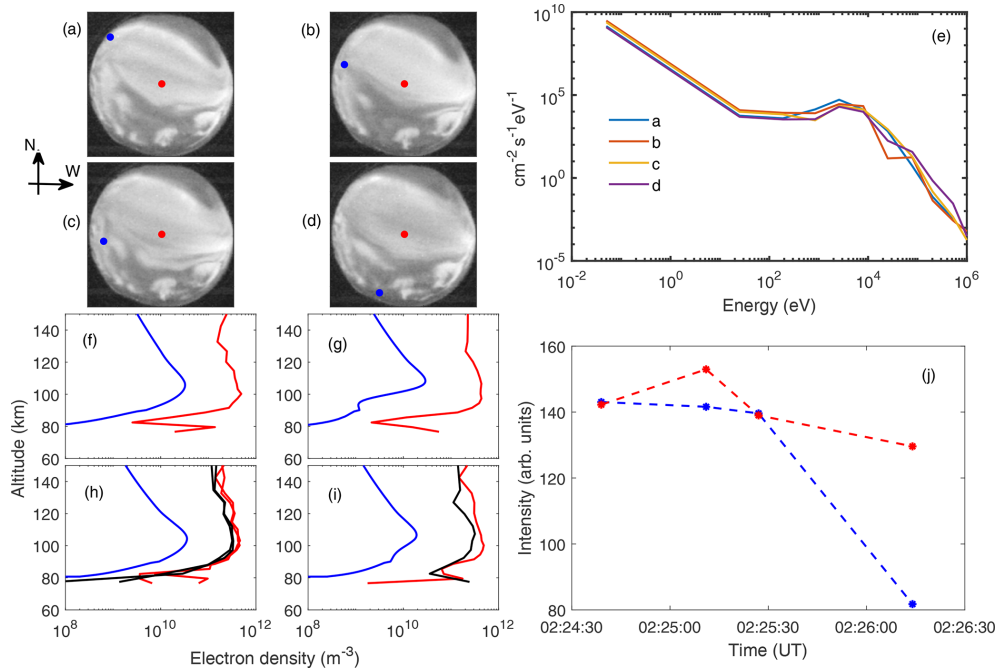


**Figure 5.** ASC images (a–d), spectra constructed from POES and the power law extrapolation (e), where the curves labeled as a–d are the corresponding spectra to the blue points on the ASC images, the model and EISCAT electron densities (f–i; colors as in Fig. 3), and the relative auroral intensities (j) at the location of the satellite measurements (blue dots) and at the EISCAT beam points (red dots), which can be found in panels (a)–(d).

ing aurora over the entire FOV of the ASC is predominantly PPA during the 1 h period; however, there are also some APA components seen in the keogram and ewogram plots. For example, before 05:15 UT, the APA type is seen in most of the ASC FOV. The ionization layer thickness also varies when the patch is visible in the EISCAT FOV (see video 3 in the Supplement). The thickness of the ionization layer around

05:25 UT is different from the thickness of the ionized layer seen just before 05:20 UT.

As shown in Fig. 7a–e, the POES measurement is not collocated with the EISCAT location; however, the structure of the PsA is the same over the ASC FOV. As is shown in Fig. 7f, the POES energy spectra is very similar in magnitude and shape in all the overpassing data points. From the ASC images (Fig. 7a–e), the EISCAT is looking in to the edge of a

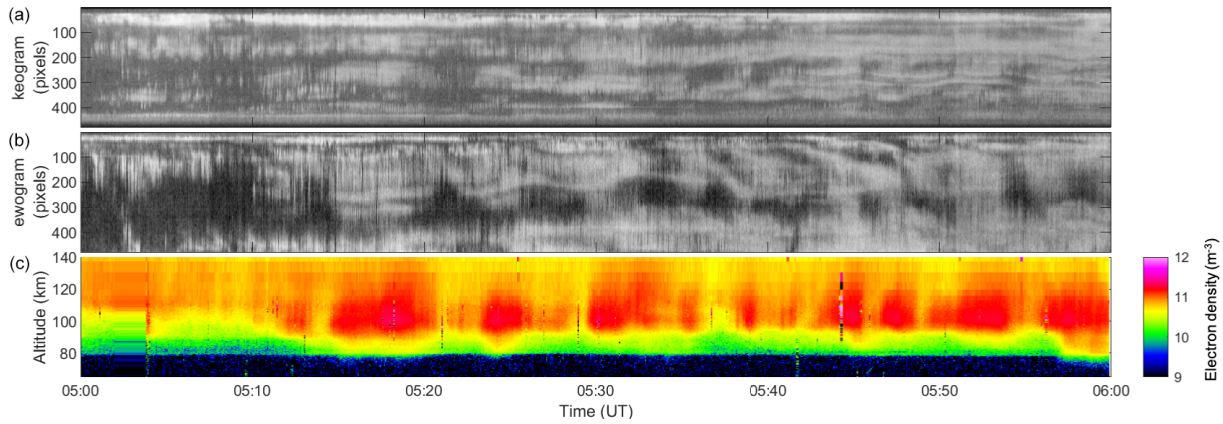


Figure 6. As in Fig. 4 but for event 3.

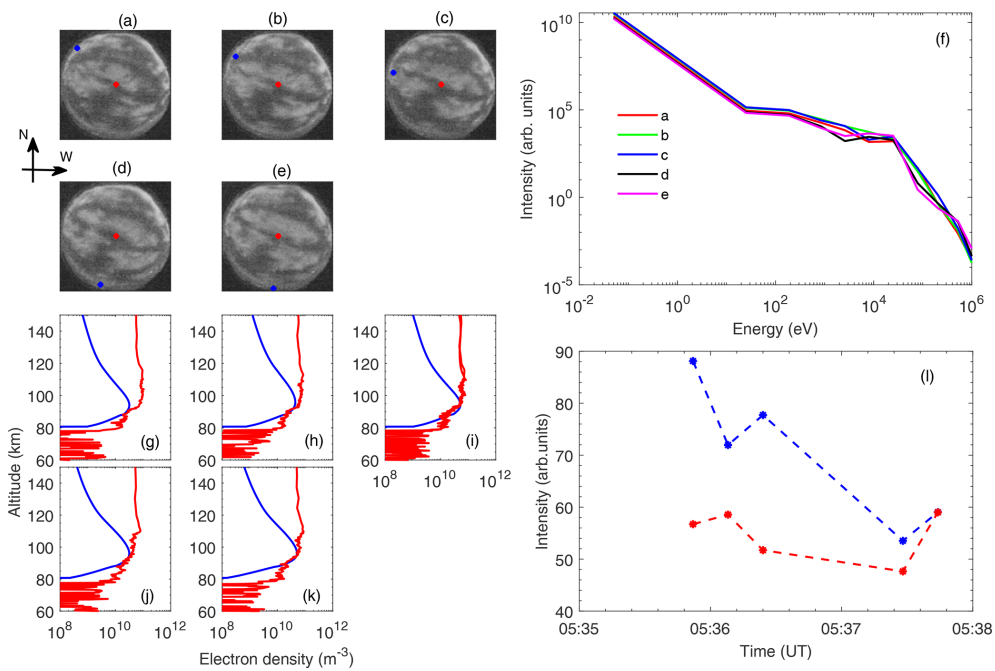


Figure 7. As in Figs. 3 and 5 but for event 3.

pulsating patch, while the POES is looking in to a patch and at the edge of a patch as it overpasses the pulsating aurora.

This event occurred very late in the morning, around 08:00 MLT (magnetic local time). A persistent structure was observed over the whole FOV of the camera for the time period where the satellite is overpassing the region. The EISCAT electron density showed constant values at 95–115 km but agrees well with the model electron density around 90 km. In Fig. 7h–k, the electron densities showed a good agreement below 105 km. However, the discrepancy between the electron densities started at an altitude of 90 km (Fig. 7g), and the electron densities below 87 km showed a significant difference (Fig. 7j–k). There is no significant increase in the fluxes at any specific energy during this whole observation

period, but the spectra rather showed a steep decrease at all the energy levels. The median auroral emission intensity showed a similar decreasing trend at both the EISCAT location and at the satellite observation point.

#### 4 Discussion

In this study, three PsA events were analyzed for their ionization characteristics. Each event analysis included high-resolution electron density measurements from the EISCAT Tromsø radar, high-resolution ASC images from the same site, and in situ particle precipitation measurements from an overpassing POES. The in situ particle spectra were used as an input to an ionospheric model, and the model results were

compared to the measured electron densities. Despite the differences between the space-borne and ground-based measurements, the conjugate measurements reveal some valuable details about the different PsA types.

Event 1 on 17 November occurred very late in the morning sector, at around 07:30 MLT, where harder precipitation is often reported to be present (Hosokawa and Ogawa, 2015). This is clearly seen in the EISCAT electron density measurements as a significant ionization below 80 km. A similar local time evolution of hardening precipitation was recently investigated by Tesema et al. (2020b) in a more statistical approach, which included EISCAT and optical data from the same geographical area. However, the cut-off altitude of the model is 80 km, which causes a large discrepancy between the model and the EISCAT electron density below 80 km. The 13 January event (event 3), which occurred about 30 min later than event 1 in local time, showed a very good agreement between the measured and modeled electron densities in the altitude range below 95 km during a softer type of precipitation. This indicates that the model is capable of reproducing measured electron densities with half an order of magnitude difference within the height region of the prompt ionization at 80–120 km and during precipitation that primarily includes particle energies which impact this height range ( $\sim 1$ –100 keV). Our conclusions are, thus, focused on interpreting the height range of 80–120 km.

In two of the three cases (both November events 1 and 2) presented in this work, the PsA category changed within the observed 1 h time period. During both events, the APA that was observed first changed into more persistent PPA. An enhancement in the measured electron density was observed at the same time, with the optical transition between the two categories as shown by vertical dashed lines in Figs. 2 and 4. Furthermore, in the November 2015 event (event 2), the POES passed over the ASC station at the time of the transition between APA and PPA types. This resulted in a big difference, of more than 1 order of magnitude, between the electron densities and in the altitude of the modeled and measured maximum electron density. In event 2, the satellite primarily measured the PPA-type precipitation, while the EISCAT radar was looking mainly into the APA-type precipitation. This suggests that a mixture of PsA types is the likely cause of the observed discrepancy.

As previously shown by a statistical analysis of the PsA type (Grono and Donovan, 2020), APA has a tendency to occur at earlier local times than PPA and PA, i.e., around and even prior to midnight. A similar order of the PsA types was found in two of our three case studies which included the transition between the different PsA types. This further suggests that the APA type may dominate the PsA events which occur during (or in between) substorm activity and predominantly undergo an increase in patch sizes during the event evolution (Partamies et al., 2019). Because these PsA events are embedded into substorm aurora, and thus would typically cover limited spatial regions compared to PA and

PPA, an overpassing spacecraft is likely to measure a mixture of different precipitation types and, thus, provide a false estimate for electron spectra at a near-conjugate ground location. However, deeper into the morning sector, where the PsA is more often PA or PPA (Grono and Donovan, 2020), the regions covered by PsA are large. In this kind of case, our findings (clearest for event 1) suggest that the overpass average of the in situ particle spectra agrees well with the ground-based measurements of electron densities. As the overpass-averaged spacecraft spectrum would necessarily include precipitation information for patches in both their on and off phases, this finding indicates that the patchiness of PsA is not a key factor in the energy deposition to the atmosphere. More detailed analysis is needed for a large number of different PsA types to confirm this result, but nonetheless, this finding may have important implications for PsA modeling studies for atmospheric chemistry impact.

## 5 Conclusions

By combining EISCAT electron density, electron precipitation measurements from POES, and model electron density outputs, we study three PsA events identified using Tromsø high-resolution ASC data. We observed different types of PsA in the three cases. We showed that the near-midnight PsA event (event 2), which includes a mix of PsA types (APA and PPA), showed a significant electron density magnitude difference between EISCAT and model outputs. The model and EISCAT electron density magnitude in the morning sector events (events 1 and 3), which consisted of measurements when the POES overpassed entirely over PPA types, showed a very good agreement in which the difference lies within half an order of magnitude. This suggests that the PsA spectra from POES used in modeling during a mix of PsA types could give an incorrect estimate if averaged spectra are used to model the energy deposition. However, the agreement during both the morning sector events indicated that overpass-averaged spectra are a very good estimate to model the PsA energy deposition without considering the patchiness of the PsA. This also indicates that the MLT dependence of PsA types might play an important role in future studies of atmospheric effects of PsA.

*Data availability.* The quick-look all-sky camera (ASC) images and keograms for the event selection are available at the Auroral Quicklook Viewer of the National Institute of Polar Research (NIPR) ground-based network (<http://pc115.seg20.nipr.ac.jp/www/AQVN/index.html>, last access: 23 December 2021). All-sky camera data are obtained upon request to the principal investigator of the auroral observation ([uapdata@nipr.ac.jp](mailto:uapdata@nipr.ac.jp)) at the NIPR. Raw EISCAT data used in this analysis are available at <http://portal.eiscat.se/schedule/schedule.cgi> (last access: 23 December 2021), and the GUISDAP (Grand Unified Incoherent Scatter Design and Analysis Package) software used to analyze the EISCAT raw data

in a high time resolution is available at <https://eiscat.se/scientist/user-documentation/guidap/> (last access: 19 December 2021).

*Author contributions.* NP helped in event selection and analysis, DKW provided the ionospheric model run, and OY helped with the analysis and provided the high-resolution all-sky camera data. All authors contributed by providing the necessary data and discussions and writing the paper.

*Competing interests.* The contact author has declared that neither they nor their co-authors have any competing interests.

*Disclaimer.* Publisher's note: Copernicus Publications remains neutral with regard to jurisdictional claims in published maps and institutional affiliations.

*Acknowledgements.* The funding support for Fasil Tesema has been provided by the Norwegian Research Council (NRC; CoE grant no. 223252). In addition, the work of Noora Partamies has been supported by NRC (project no. 287427).

*Financial support.* This research has been supported by the Norges Forskningsråd (grant nos. 223252 and 287427).

*Review statement.* This paper was edited by Dalia Buresova and reviewed by Michael Kosch and Allison Jaynes.

## References

- Berkey, F.: Observations of pulsating aurora in the day sector auroral zone, *Planet. Space Sci.*, 26, 635–650, [https://doi.org/10.1016/0032-0633\(78\)90097-1](https://doi.org/10.1016/0032-0633(78)90097-1), 1978.
- Bland, E. C., Partamies, N., Heino, E., Yukimatu, A. S., and Miyaoka, H.: Energetic Electron Precipitation Occurrence Rates Determined Using the Syowa East Super-DARN Radar, *J. Geophys. Res.-Space*, 124, 6253–6265, <https://doi.org/10.1029/2018ja026437>, 2019.
- Fukizawa, M., Sakanoi, T., Miyoshi, Y., Hosokawa, K., Shiokawa, K., Katoh, Y., Kazama, Y., Kumamoto, A., Tsuchiya, F., Miyashita, Y., Tanaka, Y. A., Kasahara, Y., Ozaki, M., Matsuoka, A., Matsuda, S., Hikishima, M., Oyama, S., Ogawa, Y., Kurita, S., and Fujii, R.: Electrostatic Electron Cyclotron Harmonic Waves as a Candidate to Cause Pulsating Auroras, *Geophys. Res. Lett.*, 45, 661–12, <https://doi.org/10.1029/2018GL080145>, 2018.
- Grono, E. and Donovan, E.: Differentiating diffuse auroras based on phenomenology, *Ann. Geophys.*, 36, 891–898, <https://doi.org/10.5194/angeo-36-891-2018>, 2018.
- Grono, E. and Donovan, E.: Surveying pulsating auroras, *Ann. Geophys.*, 38, 1–8, <https://doi.org/10.5194/angeo-38-1-2020>, 2020.
- Grono, E., Donovan, E., and Murphy, K. R.: Tracking patchy pulsating aurora through all-sky images, *Ann. Geophys.*, 35, 777–784, <https://doi.org/10.5194/angeo-35-777-2017>, 2017.
- Hosokawa, K. and Ogawa, P.: Ionospheric variation during pulsating aurora, *J. Geophys. Res.-Space*, 120, 5943–5957, <https://doi.org/10.1002/2015JA021401>, 2015.
- Jones, S. L., Lessard, M. R., Fernandes, P. A., Lummerzheim, D., Semeter, J. L., Heinselman, C. J., Lynch, K. A., Mitchell, R. G., Kintner, P. M., Stenbaek-Nielsen, H. C., and Asamura, K.: PFISR and ROPA observations of pulsating aurora, *J. Atmos. Sol.-Terr. Phys.*, 71, 708–716, <https://doi.org/10.1016/j.jastp.2008.10.004>, 2009.
- Jones, S. L., Lessard, M. R., Rychert, K., Spanswick, E., and Donovan, E.: Large-scale aspects and temporal evolution of pulsating aurora, *J. Geophys. Res.-Space*, 116, 1–7, <https://doi.org/10.1029/2010JA015840>, 2011.
- Kasahara, S., Miyoshi, Y., Yokota, S., Mitani, T., Kasahara, Y., Matsuda, S., Kumamoto, A., Matsuoka, A., Kazama, Y., Frey, H. U., Angelopoulos, V., Kurita, S., Keika, K., Seki, K., and Shinohara, I.: Pulsating aurora from electron scattering by chorus waves, *Nature*, 554, 337–340, <https://doi.org/10.1038/nature25505>, 2018.
- Lanchester, B. S., Rees, M. H., Lummerzheim, D., Otto, A., Sedgemore-Schulthess, K. J. F., Zhu, H., and McCrea, I. W.: Ohmic heating as evidence for strong field-aligned currents in filamentary aurora, *J. Geophys. Res.*, 106, 1785, <https://doi.org/10.1029/1999JA000292>, 2001.
- Lessard, M. R.: A Review of Pulsating Aurora, *Geophys. Monogr. Ser.*, 197, 55–68, <https://doi.org/10.1029/2011GM001187>, 2012.
- Lummerzheim, D. and Liliensten, J.: Electron transport and energy degradation in the ionosphere: evaluation of the numerical solution, comparison with laboratory experiments and auroral observations, *Ann. Geophys.*, 12, 1039–1051, <https://doi.org/10.1007/s00585-994-1039-7>, 1994.
- McEwen, D. J., Yee, E., Whalen, B. A., and Yau, A. W.: Electron energy measurements in pulsating auroras, *Can. J. Phys.*, 59, 1106–1115, <https://doi.org/10.1139/p81-146>, 1981.
- McKay, D., Partamies, N., and Vierinen, J.: Pulsating aurora and cosmic noise absorption associated with growth-phase arcs, *Ann. Geophys.*, 36, 59–69, <https://doi.org/10.5194/angeo-36-59-2018>, 2018.
- Miyoshi, Y., Katoh, Y., Nishiyama, T., Sakanoi, T., Asamura, K., and Hirahara, M.: Time of flight analysis of pulsating aurora electrons, considering wave-particle interactions with propagating whistler mode waves, *J. Geophys. Res.-Space*, 115, 1–7, <https://doi.org/10.1029/2009JA015127>, 2010.
- Miyoshi, Y., Oyama, S., Saito, S., Kurita, S., Fujiwara, H., Kataoka, R., Ebihara, Y., Kletzing, C., Reeves, G., Santolik, O., Clilverd, M., Rodger, C. J., Turunen, E., and Tsuchiya, F.: Energetic electron precipitation associated with pulsating aurora: EISCAT and Van Allen Probe observations, *J. Geophys. Res.-Space*, 120, 2754–2766, <https://doi.org/10.1002/2014JA020690>, 2015.
- Miyoshi, Y., Saito, S., Kurita, S., Asamura, K., Hosokawa, K., Sakanoi, T., Mitani, T., Ogawa, Y., Oyama, S., Tsuchiya, F., Jones, S. L., Jaynes, A. N., and Blake, J. B.: Relativistic Electron Microbursts as High Energy Tail of Pulsating Aurora Electrons, *Geophys. Res. Lett.*, 47, e2020GL090360, <https://doi.org/10.1029/2020gl090360>, 2020.

- Nesse Tyssøy, H., Sandanger, M. I., Ødegaard, L.-K. G., Stadsnes, J., Aasnes, A., and Zawedde, A. E.: Energetic electron precipitation into the middle atmosphere—Constructing the loss cone fluxes from MEPED POES, *J. Geophys. Res.-Space*, 121, 5693–5707, <https://doi.org/10.1002/2016JA022752>, 2016.
- Nishimura, Y., Bortnik, J., Li, W., Thorne, R. M., Lyons, L. R., Angelopoulos, V., Mende, S. B., Bonnell, J. W., Le Contel, O., Cully, C., Ergun, R., and Auster, U.: Identifying the driver of pulsating aurora, *Science*, 330, 81–84, <https://doi.org/10.1126/science.1193186>, 2010.
- Nishimura, Y., Lessard, M. R., Kato, Y., Miyoshi, Y., Grono, E., Partamies, N., Sivasdas, N., Hosokawa, K., Fukizawa, M., Samara, M., Michell, R. G., Kataoka, R., Sakanoi, T., Whiter, D. K., Oyama, S. i., Ogawa, Y., Kurita, S., ichiro Oyama, S., Ogawa, Y., and Kurita, S.: Diffuse and Pulsating Aurora, *Space Sci. Rev.*, 216, 4, <https://doi.org/10.1007/s11214-019-0629-3>, 2020.
- Ogawa, Y., Tanaka, Y., Kadokura, A., Hosokawa, K., Ebihara, Y., Motoba, T., Gustavsson, B., Brändström, U., Sato, Y., Oyama, S., Ozaki, M., Raita, T., Sigernes, F., Nozawa, S., Shiokawa, K., Kosch, M., Kauristie, K., Hall, C., Suzuki, S., Miyoshi, Y., Gerrard, A., Miyaoka, H., and Fujii, R.: Development of low-cost multi-wavelength imager system for studies of aurora and airglow, *Polar Sci.*, 23, 100501, <https://doi.org/10.1016/j.polar.2019.100501>, 2020.
- Oguti, T., Kokubun, S., Hayashi, K., Tsuruda, K., Machida, S., Kitamura, T., Saka, O., and Watanabe, T.: Statistics of pulsating auroras on the basis of all-sky TV data from five stations. I. Occurrence frequency, *Can. J. Phys.*, 59, 1150–1157, <https://doi.org/10.1139/p81-152>, 1981.
- Palmer, J.: Plasma density variations in the aurora, PhD thesis, University of Southampton, Southampton, UK, 1995.
- Partamies, N., Whiter, D., Kadokura, A., Kauristie, K., Nesse Tyssøy, H., Massetti, S., Stauning, P., and Raita, T.: Occurrence and average behavior of pulsating aurora, *J. Geophys. Res.-Space*, 122, 5606–5618, <https://doi.org/10.1002/2017JA024039>, 2017.
- Partamies, N., Bolmgren, K., Heino, E., Ivchenko, N., Borovsky, J. E., and Sundberg, H.: Patch Size Evolution During Pulsating Aurora, *J. Geophys. Res.-Space*, 124, 4725–4738, <https://doi.org/10.1029/2018JA026423>, 2019.
- Royrvik, O. and Davis, T. N.: Pulsating aurora: Local and global morphology, *J. Geophys. Res.*, 82, 4720–4740, <https://doi.org/10.1029/ja082i029p04720>, 1977.
- Tesema, F., Partamies, N., Tyssøy, H. N., Kero, A., and Smith-Johnsen, C.: Observations of electron precipitation during pulsating aurora and its chemical impact, *J. Geophys. Res.-Space*, 125, e2019JA027713, <https://doi.org/10.1029/2019JA027713>, 2020a.
- Tesema, F., Partamies, N., Tyssøy, H. N., and McKay, D.: Observations of precipitation energies during different types of pulsating aurora, *Ann. Geophys.*, 38, 1191–1202, <https://doi.org/10.5194/angeo-38-1191-2020>, 2020b.
- Turunen, E., Verronen, P. T., Seppälä, A., Rodger, C. J., Clilverd, M. A., Tamminen, J., Enell, C. F., and Ulich, T.: Impact of different energies of precipitating particles on NO<sub>x</sub> generation in the middle and upper atmosphere during geomagnetic storms, *J. Atmos. Sol.-Terr. Phys.*, 71, 1176–1189, <https://doi.org/10.1016/j.jastp.2008.07.005>, 2009.
- Turunen, E., Kero, A., Verronen, P. T., Miyoshi, Y., Oyama, S. I., and Saito, S.: Mesospheric ozone destruction by high-energy electron precipitation associated with pulsating aurora, *J. Geophys. Res.*, 121, 11852–11861, <https://doi.org/10.1002/2016JD025015>, 2016.
- Yamamoto, T.: On the temporal fluctuations of pulsating auroral luminosity, *J. Geophys. Res.*, 93, 897–911, <https://doi.org/10.1029/JA093iA02p00897>, 1988.
- Yang, B., Spanswick, E., Liang, J., Grono, E., and Donovan, E.: Responses of Different Types of Pulsating Aurora in Cosmic Noise Absorption, *Geophys. Res. Lett.*, 46, 5717–5724, <https://doi.org/10.1029/2019GL083289>, 2019.